

Article

Stability Analysis of a Vehicle–Cargo Securing System for Autonomous Trucks Based on 6-SPS-Type Parallel Mechanisms

Guosheng Zhang ¹, Tao Wang ², Han Wang ^{3,*}, Shilei Wu ⁴  and Zhongxi Shao ⁵

¹ Key Laboratory of Operation Safety Technology on Transport Vehicles, Ministry of Transport, PRC, Beijing 100088, China

² Guangdong Yueyun Traffic Rescue Co., Ltd., Guangzhou 510410, China

³ School of Mechanical Engineering, University of Shanghai for Science and Technology, Shanghai 200090, China

⁴ School of Mechanical Engineering, Suzhou University of Science and Technology, Suzhou 215009, China

⁵ School of Mechatronics Engineering, Harbin Institute of Technology, Harbin 150001, China

* Correspondence: wangh9@usst.edu.cn

Abstract: Stability prediction of the securing system for autonomous trucks is an important prerequisite for achieving safety monitoring of large cargo transportation and improving logistics efficiency. Considering the side slide risk of large cargo and the inability to predict stability using the existing under-constrained friction securing model, this paper proposes a new vehicle–cargo securing model based on the 6-SPS parallel mechanism. By establishing an analytical 3-DOF model, the dynamics performance of the vehicle–cargo system is analyzed based on the response solution under sinusoidal excitations. To verify the correctness of the analytical model, a multi-body dynamics model of the whole vehicle–cargo system based on the three-dimensional geometric model and the 6-SPS parallel mechanism is established for simulation in ADAMS. According to road class, pavement roughness is modeled by a white noise power spectrum method as the excitation in the simulation. The results show that the dynamics response of the analytical model accords well with that of the simulation model, with relative errors of 8.34% and 0.036% in amplitude and frequency, respectively. The proposed method can provide theoretical support for accurate stability prediction and for achieving safety monitoring of large cargo transportation for autonomous trucks.

Keywords: autonomous trucks; stability analysis; securing system; dynamics modeling



Citation: Zhang, G.; Wang, T.; Wang, H.; Wu, S.; Shao, Z. Stability Analysis of a Vehicle–Cargo Securing System for Autonomous Trucks Based on 6-SPS-Type Parallel Mechanisms. *Machines* **2023**, *11*, 745. <https://doi.org/10.3390/machines11070745>

Academic Editors: Zhongchao Liang, Jing Zhao and Zhongguo Li

Received: 20 June 2023

Revised: 11 July 2023

Accepted: 12 July 2023

Published: 15 July 2023



Copyright: © 2023 by the authors. Licensee MDPI, Basel, Switzerland. This article is an open access article distributed under the terms and conditions of the Creative Commons Attribution (CC BY) license (<https://creativecommons.org/licenses/by/4.0/>).

1. Introduction

Road transportation is one of the main modes of modern transportation, occupying an extremely important position in the field of transportation and playing an increasingly important role. Compared to manual transportation methods, the emergence of autonomous driving technology can improve the safety of truck driving, reduce freight transportation costs and greatly improve transportation efficiency, showing its broad application prospects [1]. However, there are still several challenges that need to be resolved in self-driving truck systems, such as precise control with complex truck system dynamics and corresponding truck-aware decision making, etc. [2]. Due to the lack of human intervention, cargo loosening, shifting, off-centered positions, and so on during transportation would negatively impact vehicle dynamics and stability and bring huge economic losses, which suggests the need for higher requirements for the stability of the securing system of autonomous trucks [3]. The stability evaluation and prediction of cargo-vehicle systems is also an important prerequisite for achieving automatic transportation safety monitoring of large cargo, as well as improving logistics efficiency by precise control.

Cargo securing methods are one of the main factors that affects stability during the transportation process. Establishing cargo securing models can help us investigate the dynamic performance of secured cargo and evaluate the applicability of different securing

methods. The classical theory of packaging dynamics was established by Mindlin et al. of Bell Laboratories, who studied the motion law of packaging products during drop impact in the case of instability [4]. Jagelčák et al. developed an over-the-top securing model and found that the trend of longitudinal movement with cargo in longitudinal movement would lead to an increase in the relative elongation of the lashing straps [5]. Dai et al. obtained tension variation data in a spacecraft cargo securing model by establishing a cargo packaging test platform, and established a tension relaxation model based on the least square method, which showed that the calculated values of the tension relaxation model were in good agreement with the measured values [6]. Zhang et al. found that the diagonal lashing method had better lateral stability when the vehicle passes through curves [7]. Turanov et al. derived the formulae for the calculation of shear forces on cargo with flexible and rigid elements fixed separately according to the geometry of fasteners [8]. With the development of dynamics and numerical computation in recent decades, the finite element method (FEM) is commonly used to establish dynamic models of cargo securing systems. Blumhardt et al. studied the change of cargo stability in the event of a collision with a truck, simulating it using the finite element method [9]. Three-dimensional (3-D) modeling of cargo was performed by Zeng et al. through the software VPG, and the corresponding finite element simulation of dynamics was performed in LS-DYNA to reveal the main factors affecting the stability of the cargo [10]. In order to study the influence of different road and vehicle conditions on cargo tying force, Zong et al. established a vehicle model and an over-the-top tying model, and obtained the acceleration values of the cargo with the simulation at normal vehicle driving speed [11]. Dong et al. derived a calculation formula of cargo oscillation caused by motion inertia force by considering the influence of dynamic parameters on the cargo vibration centerline in order to study the vibration of cargo in transit [12]. For stability analysis of cargo during transportation, Fleissner et al. proposed a method coupling Lagrangian particle methods and a multi-body system using co-simulations for the dynamic simulation of tank trucks carrying fluids and silo vehicles carrying granulates [13]. Oliveira et al. proposed a method based on mechanical equilibrium to deal with cargo stability in the container loading problem, expressed as an integer programming model [14]. Junqueira et al. proposed mixed integer linear programming methods for the container loading problem, considering vertical and horizontal stability and the load-bearing strength of the cargo [15]. Xiong et al. proposed an autonomous vehicle sideslip angle estimation algorithm based on consensus and vehicle kinematics/dynamics synthesis. Dynamics performance against the roll and pitch is measured to estimate the sideslip angle and attitude of the vehicle body [16,17]. Vlkovský et al. discussed the applicability of the key EN 12195-1:2010 standard [18] and conducted a series of comparisons to statistically analyze the impact which road surfaces have on cargo and the securing of cargo against shocks during road transport [19–21]. Transportation shocks that significantly affect the system of securing were analyzed for road safety improvement [22].

To further study cargo stability in transit, it is necessary to put the cargo, vehicle, road pavement and securing system together to establish a dynamics model of the cargo-vehicle system for comprehensive stability analysis. Elnashar et al. evaluated the effects of suspension damping and vehicle speed on flexible pavements. The vehicle was simulated as a two-degree-of-freedom quarter-vehicle model [23]. Chen et al. developed a liquid-sloshing-vehicle-dynamics-coupled model that evaluates how liquid sloshing degrades vehicle roll stability and dynamic performance [24]. Misaghi et al. presented a process to quantify the impact of truck suspension systems and road surface condition on the damage exerted to the pavement. Truck-pavement interaction models incorporated a finite element model to estimate the additional dynamic loads applied to pavements [25]. Sindha et al. compared the stability of a three-wheeled vehicle with two wheels on the front (2F1R), a three-wheeled vehicle with two wheels on the rear (1F2R) and a standard four-wheeled vehicle. Rigid body analysis was performed to find the value of a commonly used safety rating, the Static Stability Factor (SSF) of a vehicle [26].

From the above literature, it can be seen that current cargo securing standards and mechanics research are relatively mature. The construction of relevant theoretical models and simple tests have been completed in cargo stability prediction, but a perfect industry system has not yet been formed, which provides a broad research space for subsequent large cargo stability prediction technology. In addition, existing methods of cargo securing are mainly divided into support, stuffing and strapping, and are applicable for flat concrete or asphalt roads. Most suitable friction securing methods for large cargo transportation can meet the requirements of safe transportation. However, large cargoes are prone to sideslip and overturn during transportation, and friction securing methods do not limit longitudinal DOF, while longitudinal slippage leads to greater safety risks.

In view of the above problems, and considering the structural similarity between the cargo system and the 6-SPS parallel mechanism, this paper proposes a novel vehicle–cargo securing modeling method based on the 6-SPS parallel mechanism. By establishing an analytical 3-DOF model based on the 6-SPS parallel mechanism, the dynamics performance of the vehicle–cargo system is analyzed based on the response solution under sinusoidal excitations. The correctness of this analytical 3-DOF model is verified by the simulation of the corresponding multi-body dynamics model of the whole vehicle–cargo system established in ADAMS. The main contribution of this paper is that a new vehicle–cargo securing model based on the 6-SPS parallel mechanism is proposed, considering the side slide risk of large cargo and the inability to predict stability using the existing under-constrained friction securing model. The proposed modeling and analysis method can provide theoretical support for accurate stability prediction and for achieving safety monitoring of large cargo transportation for autonomous trucks.

The structure of this paper is shown in Figure 1.

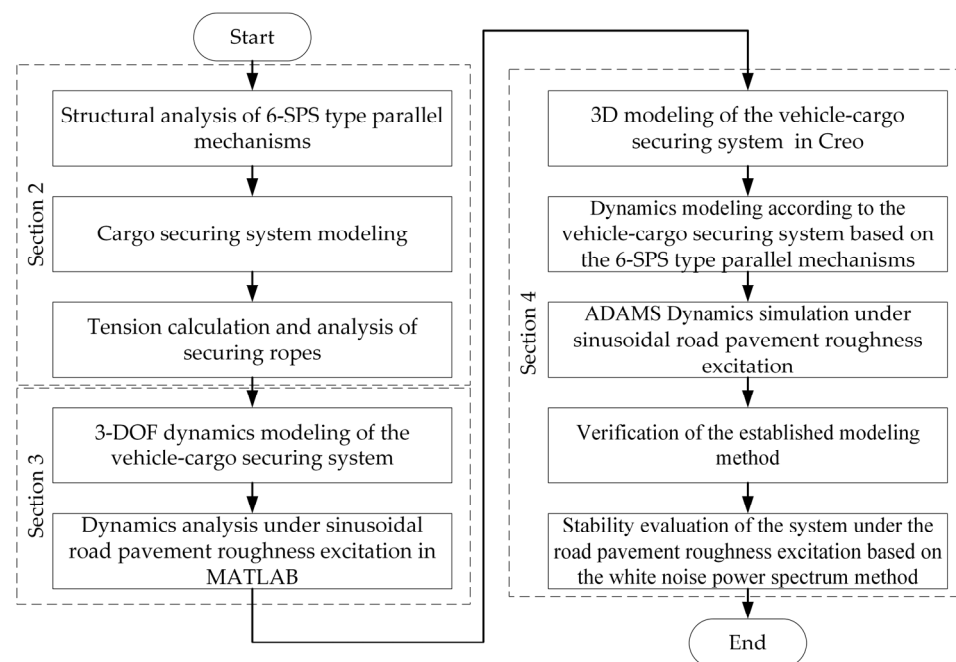


Figure 1. Holistic diagram of stability analysis of a vehicle–cargo securing system for autonomous trucks based on 6-SPS-type parallel mechanisms.

2. Cargo Securing Model Based on the 6-SPS Type Parallel Mechanism

2.1. Cargo Securing System Modeling

The cargo securing system is mainly used to fix the vertices and edges of the cargo to the platform to limit its six degrees of freedom, thus preventing the cargo from moving or overturning during transportation. Since the structure of a parallel mechanism is similar to that of a cargo securing system, a novel design, which introduces parallel mechanism modeling into the cargo securing system, is proposed.

As shown in Figure 2, a 6-SPS parallel mechanism is composed from a moving platform, a fixed platform and 6 branch chains. For the 6-SPS configuration, 6 means that the configuration consists of six links. Each link has spherical pairs (denoted by S) at its two ends and one prismatic pair (denoted by P) in the middle. $b_1 \sim b_6$ are the six connecting points of the moving platform, $B_1 \sim B_6$ are the six connecting points of the fixed platform.

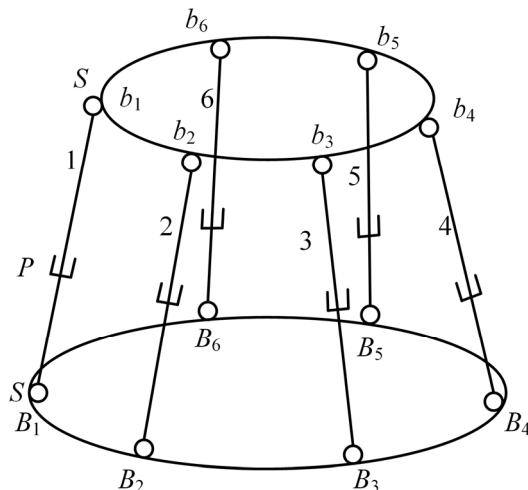


Figure 2. Diagram of the structure of a 6-SPS type parallel mechanism.

Since the 6-SPS parallel mechanism meets the structural requirements of cargo friction securing, this paper proposes a novel design for a cargo securing system using parallel mechanism modeling instead of the traditional friction securing model. In this securing system model, the moving platform of the parallel mechanism is assumed to be fixed. Considering the geometric constraints on the platform from the connecting points of the links, the cargo securing model based on the 6-SPS type parallel mechanism is shown in Figure 3.

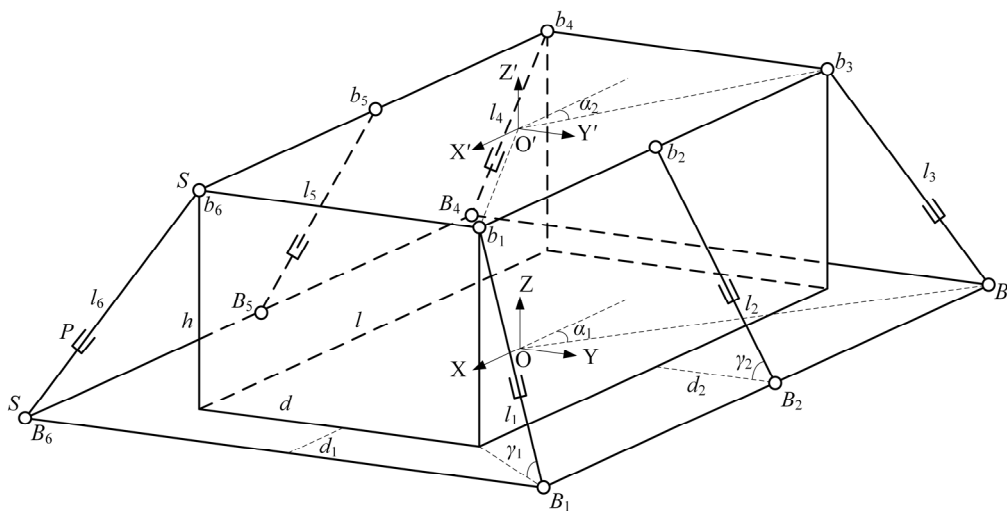


Figure 3. Cargo securing model based on the 6-SPS type parallel mechanism.

In Figure 3, $O'-X'Y'Z'$ and $O-XYZ$ are the coordinate system of the cargo (moving platform) and the coordinate system of the transportation platform (fixed platform), respectively. l , d and h are the length, width and height of the cargo. Assuming that the cargo and the platform have the same symmetric planes, d_1 and d_2 are the unilateral distances between the cargo and the platform in X and Y directions. $b_1 \sim b_6$ are the six securing points (connecting points) of the upper face of the cargo. $B_1 \sim B_6$ are the six securing points

(connecting points) of the transportation platform. $l_1 \sim l_6$ are the securing lengths of the cargo. Assume that l_1, l_3, l_4, l_6 have the same securing length l' , and the angles between the ropes (links) and the platform are γ_1 ; l_2, l_5 have the same securing length l'' , and the angles between the ropes and the platform are γ_2 . Due to oblique rope tension in the securing process, the angle between its component in the XOY plane and X-axis is γ_3 .

Based on the inverse solution of the parallel mechanism, coordinate transformation can be used to calculate each securing length in this cargo securing model. The coordinate transformation is formulated as

$$\mathbf{R} = \mathbf{TR}' \tag{1}$$

where \mathbf{R}' , \mathbf{R} and \mathbf{T} are the cargo vector in the coordinate system of the cargo, cargo vector described in the coordinate system of the transportation platform and the corresponding homogeneous transformation matrix, respectively.

The homogeneous transformation matrix from the coordinate system of the cargo to that of the transportation platform can be expressed as

$$\mathbf{T} = \begin{bmatrix} d_{11} & d_{12} & d_{13} & X_p \\ d_{21} & d_{22} & d_{23} & Y_p \\ d_{31} & d_{32} & d_{33} & Z_p \\ 0 & 0 & 0 & 1 \end{bmatrix} \tag{2}$$

where d_{ij} ($i = 1,2,3, j = 1,2,3$), X_p , Y_p , and Z_p are the rotational and translational elements of the transformation matrix.

The coordinates of each securing point, no matter on the cargo or on the transportation platform, can be calculated according to geometric relationship as

$$\begin{aligned} b_1 &= (b_{1x}, b_{1y}, 0) = (r \cos \alpha_2, r \sin \alpha_2, 0), & b_2 &= (b_{2x}, b_{2y}, 0) = (0, d/2, 0) \\ b_3 &= (b_{3x}, b_{3y}, 0) = (-r \cos \alpha_2, r \sin \alpha_2, 0), & b_4 &= (b_{4x}, b_{4y}, 0) = (-r \cos \alpha_2, -r \sin \alpha_2, 0) \\ b_5 &= (b_{5x}, b_{5y}, 0) = (0, -d/2, 0), & b_6 &= (b_{6x}, b_{6y}, 0) = (r \cos \alpha_2, -r \sin \alpha_2, 0) \end{aligned} \tag{3}$$

and

$$\begin{aligned} B_1 &= (B_{1x}, B_{1y}, 0) = (R \cos \alpha_1, R \sin \alpha_1, 0), & B_2 &= (B_{2x}, B_{2y}, 0) = (0, d/2 + d_2, 0) \\ B_3 &= (B_{3x}, B_{3y}, 0) = (-R \cos \alpha_1, R \sin \alpha_1, 0), & B_4 &= (B_{4x}, B_{4y}, 0) = (-R \cos \alpha_1, -R \sin \alpha_1, 0) \\ B_5 &= (B_{5x}, B_{5y}, 0) = (0, -d/2 - d_2, 0), & B_6 &= (B_{6x}, B_{6y}, 0) = (R \cos \alpha_1, -R \sin \alpha_1, 0) \end{aligned} \tag{4}$$

where r and R are the radii of the circumscribed circles of the cargo upper face and the transportation platform, respectively. $\alpha_1 \in [0, \pi/2]$ is the value of the azimuth angles of B_1, B_3, B_4 and B_6 with respect to the X-axis in O-XYZ. $\alpha_2 \in [0, \pi/2]$ is the value of the azimuth angles of b_1, b_3, b_4 and b_6 with respect to the X' -axis in $O'-X'Y'Z'$.

The securing length vector can be expressed in the coordinate system O-XYZ as

$$\mathbf{l}_i = \begin{bmatrix} l_{ix} \\ l_{iy} \\ l_{iz} \end{bmatrix} = \begin{bmatrix} d_{11}b_{ix} + d_{12}b_{iy} + X_p - B_{ix} \\ d_{21}b_{ix} + d_{22}b_{iy} + Y_p - B_{iy} \\ d_{31}b_{ix} + d_{32}b_{iy} + Z_p \end{bmatrix} \quad i = 1, 2, \dots, 6. \tag{5}$$

Then, the formula for calculating the securing length can be expressed as

$$l_i = \sqrt{l_{ix}^2 + l_{iy}^2 + l_{iz}^2}. \tag{6}$$

Substituting Equation (5) into Equation (6), the securing length of l_i can be obtained as

$$l_i = \sqrt{(d_{11}b_{ix} + d_{12}b_{iy} + X_p - B_{ix})^2 + (d_{21}b_{ix} + d_{22}b_{iy} + Y_p - B_{iy})^2 + (d_{31}b_{ix} + d_{32}b_{iy} + Z_p)^2}. \tag{7}$$

Based on the above derivations, the three-dimensional cargo securing model under the initial pose information in MATLAB is shown in Figure 4. The securing length data of the model are shown in Table 1.

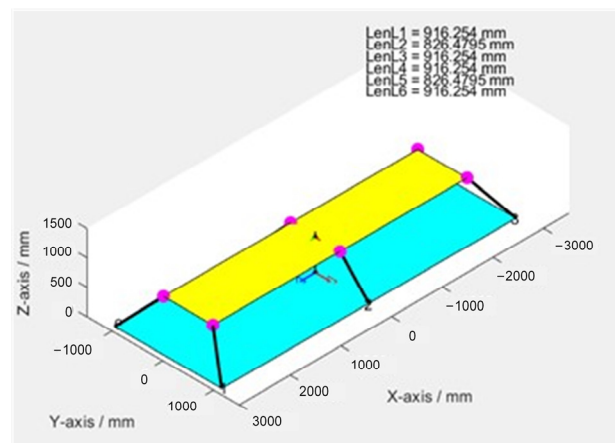


Figure 4. Three-dimensional cargo securing modeling in MATLAB.

Table 1. Securing length data of the cargo securing model.

| Rope No. | Securing Length (mm) |
|----------|----------------------|
| 1 | 916.254 |
| 2 | 826.480 |
| 3 | 916.254 |
| 4 | 916.254 |
| 5 | 826.480 |
| 6 | 916.254 |

From the securing length data in Table 1, we can calculate the corresponding angle parameters of the securing model. γ_1 , γ_2 and γ_3 can be calculated as

$$\begin{cases} \gamma_1 = \arcsin \frac{h}{l_6} \approx 40.5^\circ \\ \gamma_2 = \arcsin \frac{d_2}{l_2} \approx 41.7^\circ \\ \gamma_3 = \arccos \frac{d_1}{l_1 \cos \varphi_1} \approx 54.9^\circ \end{cases} \quad (8)$$

2.2. Tension Analysis of Securing Ropes

To ensure the safety of transportation and avoid special situations that may occur during transportation, it is necessary to make redundant designs when selecting securing rigging or ropes, to ensure that the securing riggings or ropes do not break in dangerous situations. Considering the design requirements of the cargo securing model, heavy-duty polyester ropes and corresponding binding devices are selected in this paper. The mechanical properties of polyester ropes are listed in Table 2.

Table 2. Mechanical properties of polyester ropes.

| Item | Value |
|--|------------------------|
| Fiber | Long |
| Dry fracture strength | 3.8~5.3 cN/dtex |
| Relative collusion strength | 85~100% |
| Elastic recovery rate at 3% elongation | 95~100% |
| Initial modulus | 79.2~140 cN/dtex |
| Density | 1.38 g/cm ³ |

The unit conversion formula of the initial modulus is $1 \text{ cN/dtex} = 98\rho \text{ Mpa}$ where ρ is the polyester density (g/cm³).

Taking the mean value of the polyester initial modulus, 110 cN/dtex, the elastic modulus of heavy-duty securing ropes E is

$$E = 110 \times 98 \times 1.38 = 14876.4 \text{ Mpa} \approx 14.9 \text{ Gpa} \quad (9)$$

From Table 2, it can be seen that the elastic recovery rate of polyester at 3% elongation is 95%~100%. In order to extend service life, a 1.5% elongation is selected for pre-tightening. Taking l_1 in the cargo securing model as an example, the length is 916.254 mm, and the pre-tightening length is about 13.74 mm. According to the tension calculation, the tension force F_1 is

$$F_1 = \frac{EA\Delta l_1}{l_1} = \frac{14.9 \times 10^9 \times 10^{-4} \times 0.015 \times 916.254}{916.254} \approx 22.34 \text{ kN} \quad (10)$$

where A and Δl_1 are the sectional area and the elongation of the heavy-duty securing ropes, respectively.

After calculating the pre-tightening tension force of the mooring rope, it is necessary to determine the strength of the securing ropes to prevent the pre-tightening tension from exceeding the strength and causing the securing ropes to fracture. The calculation formula for the strength S_p of the securing ropes is

$$S_p = \frac{S}{k_p k_r} = \frac{5000 \text{ g}}{2 \times 1} = 24.5 \text{ kN} \quad (11)$$

where S , k_p and k_r are the nominal load (5000 kg in this paper), the safety coefficient of polyester and the dynamic load coefficient caused by the vertical vibration acceleration, respectively. k_p and k_r are 2 and 1 in this paper.

Due to $F_1 < S_p$, which means that the tension force of the securing rope is less than its strength, the rope will not break during pre-tightening, so this pre-tightening tension is safe. After determining the pre-tightening tension, it is necessary to compare it with the pre-tightening tension in the standard. The pre-tightening tension must be greater than the pre-tightening tension in the standard to determine whether the cargo securing model is safe. The standard tension F for the securing model given in Standard EN-12195:2010 [18] is

$$F = \frac{mg(c_x - \mu f_\mu c_z)}{\cos \gamma_1 + \mu f_\mu \sin \gamma_1} = \frac{3000 \text{ g}(0.8 - 0.3)}{\cos 40.5^\circ + 0.3 \sin 40.5^\circ} \approx 15.39 \text{ kN} \quad (12)$$

where c_x , μ , f_μ and c_z are the vertical dynamic coefficient, the frictional coefficient, the conversion coefficient and the horizontal dynamic coefficient, respectively. From Equation (12), the calculated pre-tightening tension force meets the requirement of the standard, indicating the feasibility of the cargo securing model.

Based on the established cargo securing model, the vehicle is also taken into account in modeling the whole vehicle–cargo system. In this paper, a FAW Jiefang light truck is selected as the vehicle. The three-dimensional vehicle–cargo system, modeled in the commercial software Creo, is shown in Figure 5.

The vehicle–cargo system model is composed of the cargo securing model and the vehicle model. In this vehicle–cargo system model, l , d , h , γ_1 and γ_2 in Figure 5 are the same as those defined in the cargo securing model in Figure 3. G is the gravity of the whole system; v is the driving speed of the vehicle. During the transportation process, the cargo suffers from the longitudinal inertial force F_z and the transverse inertial force F_H . The pre-tensioning force F_i provided by the securing ropes can prevent the cargo from dangerous working conditions to ensure the safety of cargo transportation.

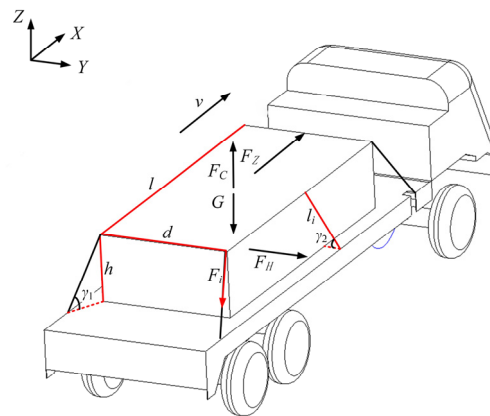


Figure 5. The three-dimensional vehicle–cargo system modeled in Creo with the diagram of the cargo securing system.

3. Dynamics Analysis of the Vehicle–Cargo Securing System

Dynamics modeling provides us with a tool to study the displacement of the cargo and the tension of the securing ropes during the transportation process, laying a foundation for the evaluation of cargo stability. In this study, a three-degree-of-freedom (3-DOF) spring-damper-mass model is used to describe the dynamics performance of the vehicle–cargo system. The dynamics model is shown in Figure 6.

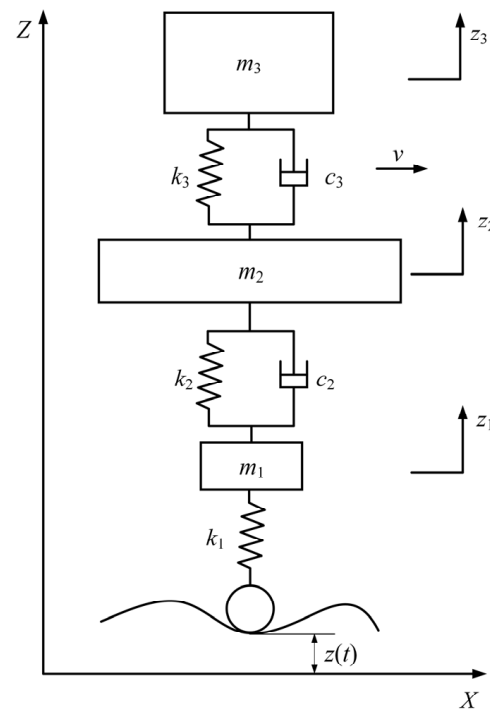


Figure 6. Diagram of the 3-DOF dynamics model of the vehicle–cargo system.

In Figure 6, m_3 is the mass of the cargo; k_3 and c_3 represent the equivalent stiffness and damping of the simplified securing ropes; m_2 is the mass of the transportation platform; k_2 and c_2 represent the equivalent stiffness and damping of the dashpot system of the vehicle; m_1 and k_1 represent the mass and stiffness of tires of the vehicle; v indicates that the vehicle drives along the positive direction of the X-axis at that speed; $z(t)$ is the input excitation from the road pavement roughness; and z_1 , z_2 and z_3 are the dynamic responses of the tires, the transportation platform and the cargo with the input excitation, respectively.

The kinetic equations of the 3-DOF dynamics model in Figure 6 can be derived as

$$\begin{cases} m_1\ddot{z}_1 + k_1z_1 + k_2(z_1 - z_2) + c_2(\dot{z}_1 - \dot{z}_2) = k_1z(t) \\ m_2\ddot{z}_2 + k_2(z_2 - z_1) + c_2(\dot{z}_2 - \dot{z}_1) + k_3z_2 + c_3\dot{z}_2 = 0 \\ m_3\ddot{z}_3 + k_3(z_3 - z_2) + c_3(\dot{z}_3 - \dot{z}_2) = 0 \end{cases} \quad (13)$$

To simplify the calculation process, Equation (13) is rewritten in the form of matrices:

$$\begin{bmatrix} m_1 & 0 & 0 \\ 0 & m_2 & 0 \\ 0 & 0 & m_3 \end{bmatrix} \begin{bmatrix} \ddot{z}_1 \\ \ddot{z}_2 \\ \ddot{z}_3 \end{bmatrix} + \begin{bmatrix} c_2 & -c_2 & 0 \\ -c_2 & c_2 + c_3 & 0 \\ 0 & -c_3 & c_3 \end{bmatrix} \begin{bmatrix} \dot{z}_1 \\ \dot{z}_2 \\ \dot{z}_3 \end{bmatrix} + \begin{bmatrix} k_1 + k_2 & -k_2 & 0 \\ -k_2 & k_2 + k_3 & 0 \\ 0 & -k_3 & k_3 \end{bmatrix} \begin{bmatrix} z_1 \\ z_2 \\ z_3 \end{bmatrix} = \begin{bmatrix} k_1z(t) \\ 0 \\ 0 \end{bmatrix}. \quad (14)$$

The road pavement roughness excitation is simplified to a sinusoidal input, the expression of which is

$$z(t) \approx B_0 \sin \omega t = B_0 \sin \frac{2\pi v}{\lambda} t \quad (15)$$

where B_0 , v and λ are the amplitude of road pavement roughness excitation, the speed of the vehicle and the wavelength of road pavement roughness excitation, respectively.

Most differential equations are very difficult to solve, since second-order derivatives and first-order derivatives exist simultaneously. The Fourier transform can greatly simplify the complexity of the differential equation by transforming the relevant parameters from the time domain to the frequency domain, eliminating the structure associated with second-order derivatives and first-order derivatives. Therefore, the Fourier transform is used in solving all differential equations, which can be expressed as

$$\begin{bmatrix} m_1 & 0 & 0 \\ 0 & m_2 & 0 \\ 0 & 0 & m_3 \end{bmatrix} \begin{bmatrix} (i\omega)^2 Z_1 \\ (i\omega)^2 Z_2 \\ (i\omega)^2 Z_3 \end{bmatrix} + \begin{bmatrix} c_2 & -c_2 & 0 \\ -c_2 & c_2 + c_3 & 0 \\ 0 & -c_3 & c_3 \end{bmatrix} \begin{bmatrix} i\omega Z_1 \\ i\omega Z_2 \\ i\omega Z_3 \end{bmatrix} + \begin{bmatrix} k_1 + k_2 & -k_2 & 0 \\ -k_2 & k_2 + k_3 & 0 \\ 0 & -k_3 & k_3 \end{bmatrix} \begin{bmatrix} Z_1 \\ Z_2 \\ Z_3 \end{bmatrix} = \begin{bmatrix} k_1 Z_0 \\ 0 \\ 0 \end{bmatrix}. \quad (16)$$

Taking Z_i in Equation (16) as the Fourier transform of z_i ($i = 0, 1, 2, 3$), the expression can be solved using Kramer’s rule:

$$Z_1 = \frac{D_1}{D}, Z_2 = \frac{D_2}{D}, Z_3 = \frac{D_3}{D} \quad (17)$$

where D , D_1 , D_2 and D_3 are expressed by Equations (18)–(21), respectively.

$$D = \begin{vmatrix} -\omega^2 m_1 + i\omega c_2 + k_1 + k_2 & -i\omega c_2 - k_2 & 0 \\ -i\omega c_2 - k_2 & -\omega^2 m_2 + i\omega(c_2 + c_3) + k_2 + k_3 & 0 \\ 0 & -i\omega c_3 - k_3 & -i\omega^2 m_3 + i\omega c_3 + k_3 \end{vmatrix}, \quad (18)$$

$$D_1 = \begin{vmatrix} k_1 Z_0 & -i\omega c_2 - k_2 & 0 \\ 0 & -\omega^2 m_2 + i\omega(c_2 + c_3) + k_2 + k_3 & 0 \\ 0 & -i\omega c_3 - k_3 & -i\omega^2 m_3 + i\omega c_3 + k_3 \end{vmatrix}, \quad (19)$$

$$D_2 = \begin{vmatrix} -\omega^2 m_1 + i\omega c_2 + k_1 + k_2 & k_1 Z_0 & 0 \\ -i\omega c_2 - k_2 & 0 & 0 \\ 0 & 0 & -i\omega^2 m_3 + i\omega c_3 + k_3 \end{vmatrix}, \quad (20)$$

and

$$D_3 = \begin{vmatrix} -\omega^2 m_1 + i\omega c_2 + k_1 + k_2 & -i\omega c_2 - k_2 & k_1 Z_0 \\ -i\omega c_2 - k_2 & -\omega^2 m_2 + i\omega(c_2 + c_3) + k_2 + k_3 & 0 \\ 0 & -i\omega c_3 - k_3 & 0 \end{vmatrix}. \quad (21)$$

The solutions of the Fourier transform equations are all in the frequency domain. To obtain the dynamic response of the cargo securing model during the transportation process, the solution needs to be re-transformed from the frequency domain to the time domain.

The Fourier inverse transform of the above equation solves the displacement response of the cargo under the sinusoidal road pavement roughness excitation as

$$z_3 = A_3 \sin(\omega_3 t + \varphi_3) \quad (22)$$

where A_3 , φ_3 and θ_3 are expressed as

$$A_3 = \left| \frac{k_1(k_2 + \omega c_2)(k_3 + \omega c_3)}{D} \right|, \quad (23)$$

$$\varphi_3 = \theta + \tan^{-1} \left(\frac{\omega c_2}{-\omega^2 m_2 + k_2} \right), \quad (24)$$

and

$$\theta_3 = \tan^{-1}(c_1 \omega / k_1). \quad (25)$$

Similarly, the displacement responses of the tires and the transportation platform can also be expressed as

$$\begin{cases} z_1 = A_1 \sin(\omega_1 t + \varphi_1) \\ z_2 = A_2 \sin(\omega_2 t + \varphi_2) \end{cases}. \quad (26)$$

Thus, the kinetic energy of the 3-DOF vehicle–cargo system under the sinusoidal road pavement roughness excitation is

$$E_k = \frac{1}{2} m_1 \dot{z}_1^2 + \frac{1}{2} m_2 \dot{z}_2^2 + \frac{1}{2} m_3 \dot{z}_3^2. \quad (27)$$

After obtaining the displacement response of the cargo from the 3-DOF system dynamics model, the securing tension can be calculated by combining the response with the equivalent stiffness of the securing ropes. This calculated result can help us determine whether or not the securing tension caused by the road pavement roughness excitation is greater than the allowable tension of the ropes, preventing the structure of the securing model from instability and ensuring the safety of cargo transportation.

The simulation of the 3-DOF system dynamics model can verify the accuracy of the cargo response and provide technical support for the analysis of the dynamic characteristics of the system. The parameter settings in this simulation are listed in Table 3.

Table 3. Parameter settings in the simulation of dynamic displacement response.

| Parameter | Value |
|--------------------------------|-------------------------|
| m_3 | 3 t |
| k_3 | 8×10^4 N/m |
| c_3 | 1.2×10^3 N·s/m |
| F_i ($i = 1, 2, \dots, 6$) | 22.34 kN |
| m_2 | 4 t |
| k_2 | 265 kN/m |
| c_2 | 4.2 kN·s/m |
| m_1 | 30 kg |
| k_1 | 400 kN/m |

After parameter initialization of the system, the dynamic displacement response curves of vehicle tires, transport platform and cargo displacement under sinusoidal road pavement roughness excitation can be plotted in the MATLAB simulation as shown in Figures 7–9. The displacement responses are solved by the ode45 function, which is a numerical solution provided in MATLAB. The amplitude and frequency of the displacement response of the cargo solved by the numerical method is 0.0545 mm and 0.332 Hz.

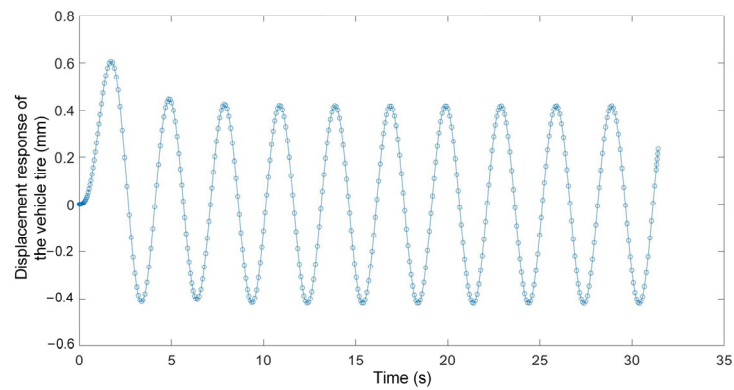


Figure 7. Displacement response curve of vehicle tires.

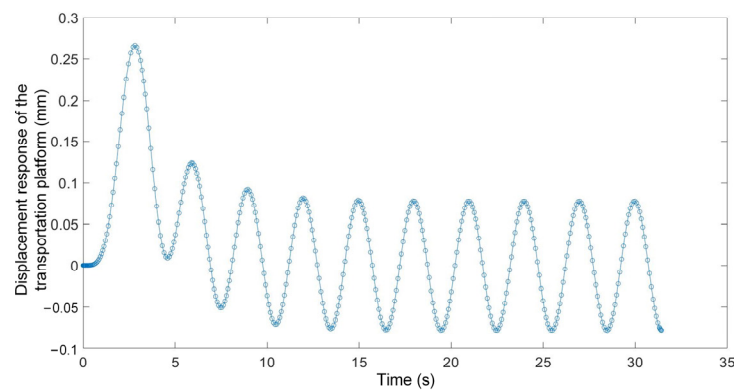


Figure 8. Displacement response curve of the transportation platform.

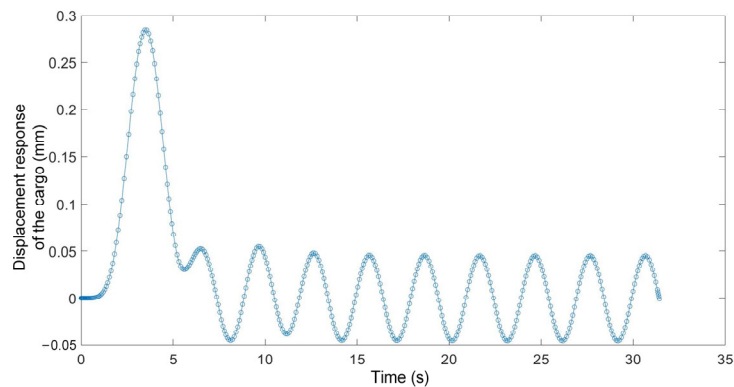


Figure 9. Displacement response curve of the cargo.

From Figures 7–9, all the displacement responses are sinusoidal at steady state under the sinusoidal road pavement roughness excitation, which indicates that the calculation of the displacement responses for the whole 3-DOF system works well in MATLAB. Plotting the above three curves within the same coordinate system, the displacement responses of the vehicle–cargo system can be obtained, as shown in Figure 10.

It can be seen from Figure 10 that the sinusoidal excitation of road pavement roughness is transferred from the tires to the cargo, and the vibration amplitude of the cargo is gradually reduced to 0.0545 mm by the dashpot system (dampers), which indicates that the damping effect of the proposed securing model based on the 6-SPS type parallel mechanisms is as expected and can meet the transportation demand of large cargo.

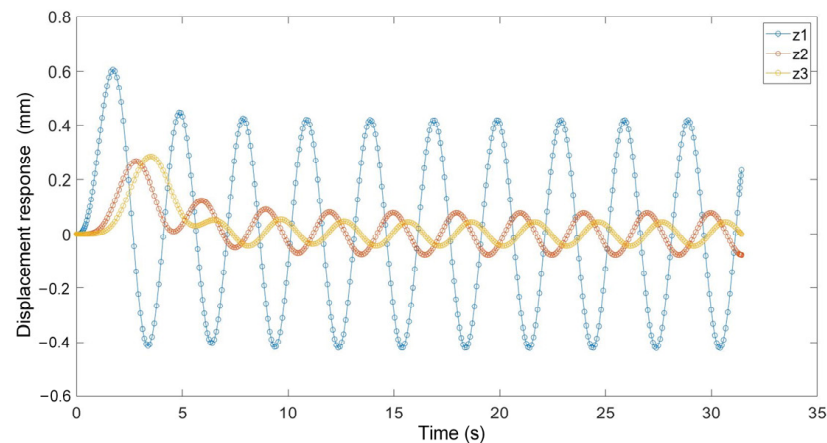


Figure 10. The displacement responses of the vehicle–cargo system.

4. Stability Analysis of Vehicle–Cargo Securing System

In order to monitor the situation of large cargo in real-time to avoid the structural instability of the vehicle–cargo system, this paper establishes a time-domain model of road pavement roughness based on the white noise power spectrum method as the input of the securing simulation. The commercial software ADAMS is used to simulate and analyze the stability of the vehicle–cargo securing system based on the 6-SPS type parallel mechanism. The established virtual model of the whole vehicle–cargo securing system, including the road pavement (modeled as two planes), is shown in Figure 11.

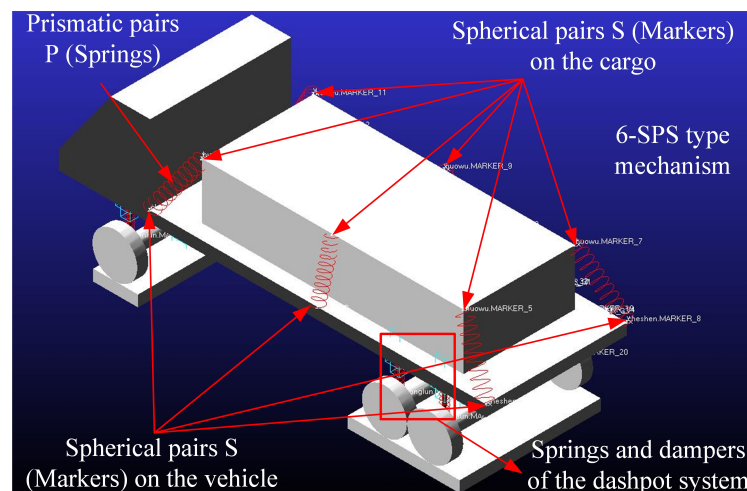


Figure 11. Virtual model of the whole vehicle–cargo securing system, with cargo securing system, in ADAMS.

Considering the complexity of the excitation from the actual road during the driving process, the model used to describe road pavement roughness should be simplified in the dynamics analysis of the vehicle–cargo securing system. Due to the fact that the natural frequency of the vehicle and the wheels are generally between 1~2 Hz and 10~15 Hz, the frequency range of the pavement roughness excitation is thus selected as not less than 15 Hz or not bigger than 1 Hz in this paper. According to the common road specified by A~C classes, the average height difference of pavement roughness is 0.5 mm, so the input sinusoidal excitation amplitude from road pavement roughness is set to 0.5 mm in this simulation. The sinusoidal excitation frequency of road pavement roughness is set to 0.33 Hz. The excitation curve of road pavement roughness is plotted as shown in Figure 12.

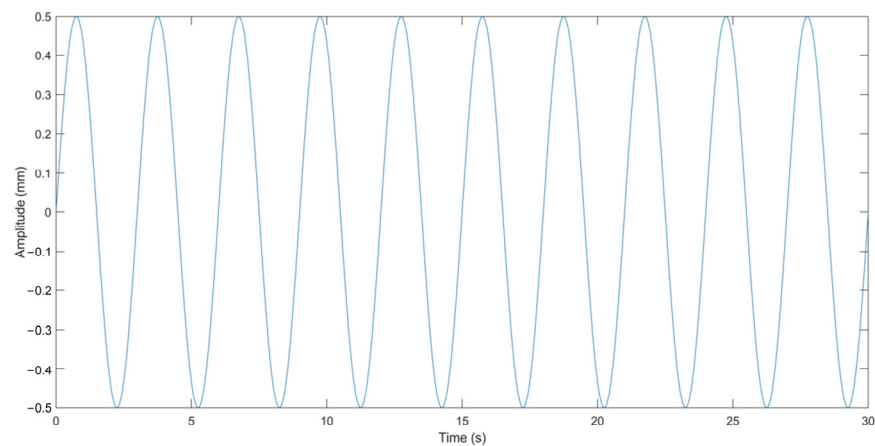


Figure 12. Sinusoidal excitation of road pavement roughness.

Importing the above excitation into the road pavement models (two plates) in ADAMS, the displacement response curve of the cargo is output as shown in Figure 13. It is noted that, according to the established 3-DOF dynamics model, only the dynamics performance of vertical movement of the vehicle–cargo system is considered in this work. Due to the DOF difference between the dynamics models established in MATLAB and in ADAMS, road pavement roughness excitations are applied with the same amplitude, frequency and phase to the two plates in ADAMS, avoiding the consideration of the influence on the other DOFs, such as roll and pitch.

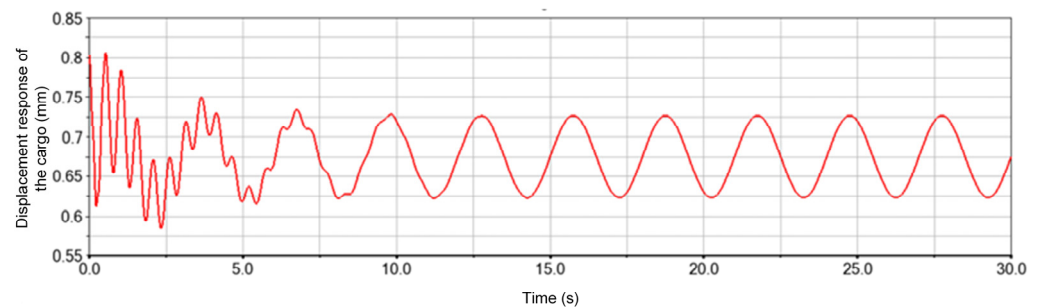


Figure 13. Displacement response curve of the cargo under sinusoidal excitation.

The simulation result shows that under the sinusoidal excitation of road pavement roughness, the displacement response curve of the cargo simulated by ADAMS is sinusoidal, as well as the numerical solution calculated by the dynamics equations in MATLAB. The ADAMS simulation result is slightly larger than the numerical solutions produced by MATLAB, and the differences in amplitude and frequency are 8.34% and 0.0364%, respectively. It is indicated that the proposed vehicle–cargo securing system based on 6-SPS type parallel mechanisms is reasonable, and the 3D structural model in ADAMS is also consistent with the dynamics model.

Based on the white noise power spectrum method, an excitation model of road pavement roughness is established as the external input of the model to investigate the stability of the whole system in the simulation. To ensure the stability of the cargo securing model under harsh road conditions, a class E road is chosen to determine road pavement roughness, and the vehicle driving speed is 60 km/h. The time-varied displacement response curves of the cargo and the transportation platform, the securing rope tension curve of l_2/l_5 and the kinetic energy curve of the cargo are plotted in Figures 14–16.

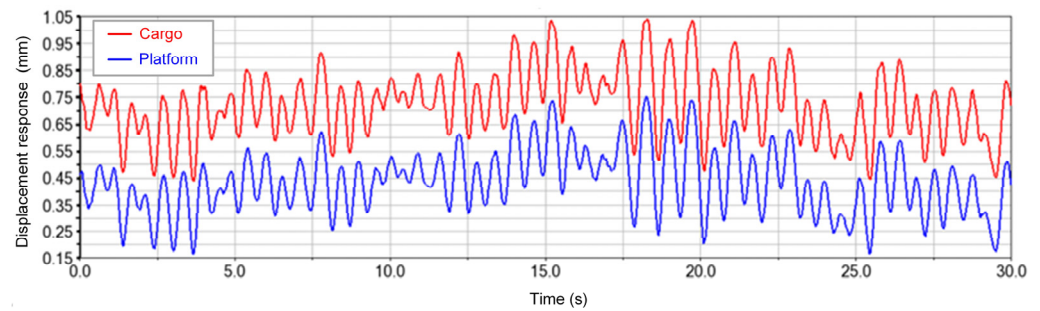


Figure 14. Displacement response curves of the cargo and the transportation platform under class E road pavement roughness excitation based on the white noise power spectrum method.

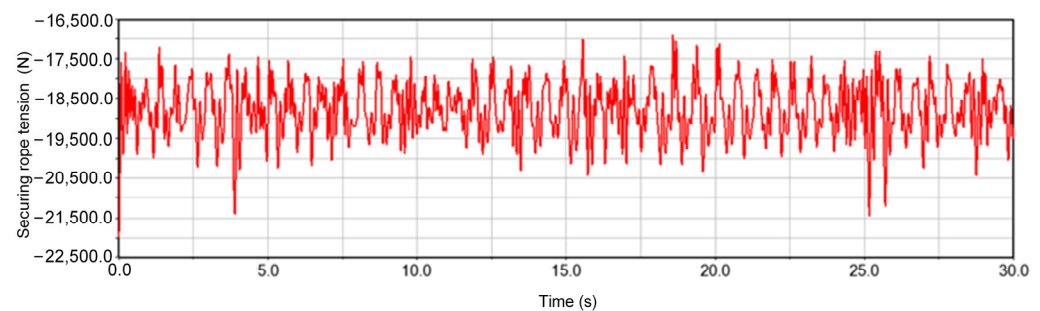


Figure 15. Tension curve of securing rope l_2/l_5 under class E road pavement roughness excitation based on the white noise power spectrum method.

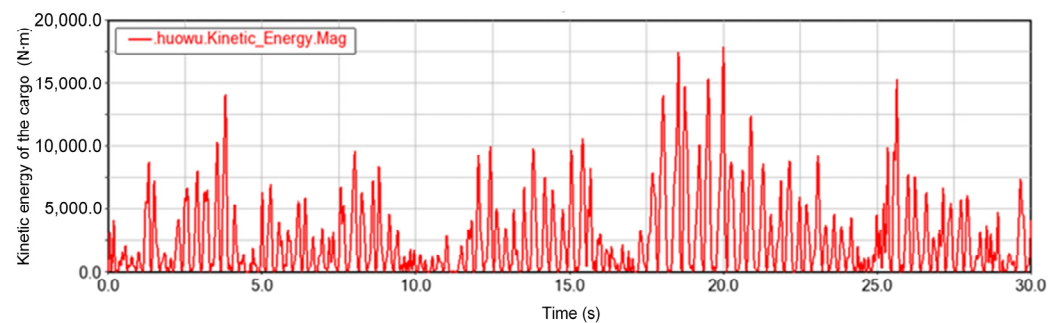


Figure 16. Kinetic energy curve of the cargo under class E road pavement roughness excitation based on the white noise power spectrum method.

In Figure 14, the curves in red and blue represent the dynamic displacement responses of the cargo and the transportation platform, respectively. The difference between these two curves always remains at a fixed value, indicating that the stability of the proposed cargo securing structure is good, and for this vehicle–cargo securing system, dangerous working conditions such as deflection and overturning will not occur during the transportation process, meeting the requirements of safe transportation.

Based on the 3-DOF analytical dynamics model, dynamics performance along vertical movement is analyzed, which means that l_2 and l_5 have the largest tension force under the same amplitude of vertical displacement response. From Figure 15, it is seen that the tension values of the securing ropes fluctuate within a range from 17.5 kN to 20.5 kN, and the maximum reaches 21.5 kN, less than the safety threshold of the securing ropes, whose maximum allowable tension is 22.34 kN. It is indicated that the securing ropes have the capability for large cargo transportation and will not break when suffering from the given road pavement roughness excitation during the transportation process.

The maximum of cargo kinetic energy in Figure 16 is about 17.5 kN·m, and it occurs when the amplitude of road pavement roughness reaches maximum. It is indicated that

road pavement roughness can affect the stability of cargo transportation to a large extent. Therefore, the securing model or securing method for large cargo transportation should be designed redundantly, according to the maximum amplitude of road pavement roughness to guarantee the flexible operation of the vehicle–cargo system, making it suitable for various harsh road conditions. Further, based on this study, the tension force data of the securing ropes, which monitor the state of the cargo, can be captured by sensors and input into the control system of autonomous trucks for decision-making during the transportation process.

5. Conclusions

This paper proposes a new vehicle–cargo securing model based on the 6-SPS parallel mechanism to guarantee large cargo transportation stability for autonomous trucks. A three-dimensional model of the vehicle–cargo system was established in Creo. A 3-DOF dynamics model of the vehicle–cargo system was also established and the corresponding displacement response equations derived. Based on the simulation of the 3-DOF vehicle–cargo system in MATLAB, the dynamic displacement response of the cargo was 0.0545 mm, indicating that the securing system has an expected damping effect. According to the ADAMS simulation result based on a structural model of the vehicle–cargo system, the difference between the dynamic displacement responses of the cargo and the transportation platform always remains at a fixed value. The tension values of the securing ropes fluctuated within a range from 17.5 kN to 20.5 kN, less than the safety threshold of the securing ropes. The proposed modeling method can provide theoretical support for accurate stability prediction and achieving safety monitoring of large cargo transportation for autonomous trucks.

Author Contributions: Conceptualization, G.Z. and H.W.; methodology, G.Z.; software, T.W.; validation, G.Z.; formal analysis, G.Z.; writing—original draft preparation, G.Z.; writing—review and editing, H.W. and T.W.; visualization, S.W.; supervision, H.W.; project administration, Z.S.; funding acquisition, Z.S. All authors have read and agreed to the published version of the manuscript.

Funding: This work is supported by the Opening Project of Key Laboratory of Operation Safety Technology on Transport Vehicles, Ministry of Transport, PRC (grant no. 2020-8409).

Institutional Review Board Statement: The study did not require ethical approval.

Informed Consent Statement: Not applicable.

Data Availability Statement: Not applicable.

Conflicts of Interest: The authors declare no conflict of interest.

References

1. Loske, D.; Klumpp, M. Intelligent and efficient? An empirical analysis of human-AI collaboration for truck drivers in retail logistics. *Int. J. Logist. Manag.* **2021**, *4*, 32. [[CrossRef](#)]
2. Wang, D.; Gao, L.; Lan, Z.; Li, W.; Ren, J.; Zhang, J.; Zhang, P.; Zhou, P.; Wang, S.; Pan, J.; et al. An intelligent self-driving truck system for highway transportation. *Front. Neurobotics* **2022**, *16*, 843026. [[CrossRef](#)] [[PubMed](#)]
3. Chen, Y.; Zheng, X.; Zhang, Z.; Ahmadian, M. Effect of off-centred loading on roll stability of multi-trailer trucks. *Int. J. Veh. Perform.* **2022**, *8*, 271–295. [[CrossRef](#)]
4. Mindlin, R.D. Dynamics of Package Cushioning. *Bell Syst. Tech. J.* **1945**, *24*, 353–461. [[CrossRef](#)]
5. Jagelčák, J.; Saniga, J. Analysis of elongation of lashing straps on movements of cargo secured by a top-over lashing at sliding in longitudinal direction. *Load Restrain. Road Veh. Saf.* **2013**, *2*, 53–62.
6. Dai, H.; Yuan, W.; Du, R.; Dong, L. Relaxation characteristics and modeling of cargo package binding in cargo spacecraft. *IOP Conf. Ser. Mater. Sci. Eng.* **2018**, *392*, 062029. [[CrossRef](#)]
7. Zhang, D.; Tang, Y.; Clarke, D.B.; Peng, Q.; Dong, C. An innovative method for calculating diagonal lashing force of cargo on railway wagons in a curve alignment. *Veh. Syst. Dyn.* **2019**, *11*, 352–374. [[CrossRef](#)]
8. Turanov, K.; Ruzmetov, Y.; Shikhnazarov, J. Incorrectness of the method of calculating cargo fastening on railway platforms. In Proceedings of the E3S Web of Conferences, Topical Problems of Green Architecture, Civil and Environmental Engineering, TPACEE 2019, Moscow, Russia, 20–22 November 2019; Volume 164, p. 03040.
9. Blumhardt, R. FEM-crash simulation and optimization. *Int. J. Veh. Des.* **2001**, *26*, 331–347. [[CrossRef](#)]

10. Zeng, X. Research of frontal energy-absorbing structure of light truck. *Mod. Manuf. Eng.* **2012**, *8*, 36–40.
11. Zong, C.; Zhang, H.; Huang, C.; Dong, J. Research on the influence of cargo securing force with typical road alignments and vehicle working conditions. In Proceedings of the 2017 4th International Conference on Transportation Information and Safety, Banff, AB, Canada, 8–10 August 2017; pp. 27–32.
12. Dong, M.; Wang, J.; Pang, B.; Wang, S. Maximum oscillation amplitude of cargo caused by inertia forces for tower cranes. In Proceedings of the International Conference on Education, Management, Computer and Society, Shenyang, China, 1–3 January 2016; pp. 1410–1413.
13. Fleissner, F.; Lehnart, A.; Eberhard, P. Dynamic simulation of sloshing fluid and granular cargo in transport vehicles. *Veh. Syst. Dyn.* **2010**, *48*, 3–15. [[CrossRef](#)]
14. Oliveira, L.A.; Lima, V.L.; Queiroz, T.; Miyazawa, F.K. The container loading problem with cargo stability: A study on support factors, mechanical equilibrium and grids. *Eng. Optim.* **2020**, *12*, 1192–1211. [[CrossRef](#)]
15. Junqueira, L.; Morabito, R.; Yamashita, D.S. Three-dimensional container loading models with cargo stability and load bearing constraints. *Comput. Oper. Res.* **2012**, *39*, 74–85. [[CrossRef](#)]
16. Xiong, L.; Xia, X.; Lu, Y.; Liu, W.; Gao, L.; Song, S.; Yu, Z. IMU-based automated vehicle body sideslip angle and attitude estimation aided by GNSS using parallel adaptive Kalman filters. *IEEE Trans. Veh. Technol.* **2020**, *69*, 10668–10680. [[CrossRef](#)]
17. Xia, X.; Hashemi, E.; Xiong, L.; Khajepour, A. Autonomous vehicle kinematics and dynamics synthesis for sideslip angle estimation based on consensus Kalman filter. *IEEE Trans. Contr. Syst. Technol.* **2023**, *31*, 179–192. [[CrossRef](#)]
18. EN 12195-1:2010; Lod Restraining on Road Vehicles-Safety-Part 1: Calculation of Securing Forces. European Committee for Standardization: Brussels, Belgium, 2010. Available online: <https://standards.iteh.ai/catalog/standards/cen/72067d57-b90c-4ca5-8bd0-f876e25e6a6e/en-12195-1-2010> (accessed on 20 June 2023).
19. Vlkovský, M.; Veselík, P. Cargo securing—Comparison of different quality roads. *Acta Univ. Agric. Silvic. Mendel. Brun.* **2019**, *67*, 1015–1023. [[CrossRef](#)]
20. Vlkovský, M.; Vlachova, H. Securing cargo during transport on roads of different quality. In Proceedings of the International Conference on Vehicle Technology and Intelligent Transport Systems, Heraklion, Greece, 3–5 May 2019; pp. 25–32.
21. Vlkovský, M. Impact of vehicle type and road quality on cargo securing. *Komunikacie* **2020**, *22*, 9–14. [[CrossRef](#)]
22. Vlkovský, M.; Neubauer, J.; Malíšek, J.; Michálek, J. Improvement of road safety through appropriate cargo securing using outliers. *Sustainability* **2021**, *13*, 2688. [[CrossRef](#)]
23. Elnashar, G.; Bhat, R.B.; Sedaghati, R. Modeling and dynamic analysis of a vehicle-flexible pavement coupled system subjected to road surface excitation. *J. Mech. Sci. Technol.* **2019**, *33*, 3115–3125. [[CrossRef](#)]
24. Chen, Y.; Ahmadian, M. Countering the destabilizing effects of shifted loads through pneumatic suspension design. *SAE Int. J. Veh. Dyn. Stab. NVH* **2019**, *4*, 5–17. [[CrossRef](#)]
25. Misaghi, S.; Tirado, C.; Nazarian, S.; Carrasco, C. Impact of pavement roughness and suspension systems on vehicle dynamic loads on flexible pavements. *Transp. Eng.* **2021**, *3*, 100045. [[CrossRef](#)]
26. Sindha, J.; Chakraborty, B.; Chakravarty, D. Rigid body modeling of three wheel vehicle to determine the dynamic stability—A practical approach. In Proceedings of the 2015 IEEE International Transportation Electrification Conference (ITEC) IEEE, Chennai, India, 27–29 August 2015.

Disclaimer/Publisher’s Note: The statements, opinions and data contained in all publications are solely those of the individual author(s) and contributor(s) and not of MDPI and/or the editor(s). MDPI and/or the editor(s) disclaim responsibility for any injury to people or property resulting from any ideas, methods, instructions or products referred to in the content.